Acousto-optic-assisted diffuse optical tomography

Aliaksandr Bratchenia,[1,*] Robert Molenaar,[2] Ton G. van Leeuwen,[1,3] and Rob P.H. Kooyman[2]

[1]*Biomedical Photonic Imaging Group, Faculty of Science and Technology, MIRA Institute for Biomedical Technology and Technical Medicine, University of Twente, P.O. Box 217, 7500AE Enschede, the Netherlands*

[2]*Nano Biophysics Group, Faculty of Science and Technology, MIRA Institute for Biomedical Technology and Technical Medicine, University of Twente, P.O. Box 217, 7500AE Enschede, the Netherlands*

[3]*Biomedical Engineering & Physics, Academic Medical Center, University of Amsterdam, P.O. Box 22700, 1100 DE Amsterdam, the Netherlands*

**Corresponding author: a.bratchenia@tnw.utwente.nl*

Received December 20, 2010; revised March 23, 2011; accepted March 26, 2011; posted March 30, 2011 (Doc. ID 139812); published April 20, 2011

We introduce and experimentally demonstrate acousto-optic-assisted diffuse optical tomography (DOT) using a holography-based acousto-optic setup. The method is based on probing a scattering medium with a localized acoustical modulation of the phase of the scattered light. The optical properties of the scattering medium are recovered with ultrasound-limited resolution by applying DOT reconstruction methods on a set of the measured intensities of light, modulated at different locations throughout the medium.

OCIS codes: 110.6960, 170.1065, 170.6510, 170.6960.

Imaging modalities, capable of probing deep into biomedical tissue, are of increasing importance. Optical methods, with virtues such as relatively low cost, the ability to detect particular compounds on the basis of their specific optical spectra, and the use of harmless light (at moderate intensities), are hampered by the scattering of light by human tissue. Consequently, localization of specific structures using light only, e.g., to visualize blood vessels deeper than a few millimeters under the skin, is difficult. Owing to the reduced scattering of ultrasound (US) by tissue, the combination of US with light can circumvent this problem. In photoacoustics, a US pulse is generated by a laser pulse. The origin of this US pulse, located at a volume with relatively high optical absorption, can be well localized, whereas the quantification of the local light absorption coefficients is difficult [1]. In acousto-optics [2,3], the colocalization (in space and time) of US pulses and light induces a frequency shift of the light with the US frequency. Detection of this modulated light allows thus exclusive measurement of the light that traveled through this tissue volume. In a previous experiment, based on calibration procedures and using a model system, we have indeed shown that local (optical) absorption coefficients can be obtained, albeit under relatively strict conditions on size and number of optical inhomogeneities [4,5]. In this communication, we show that acousto-optic-assisted diffuse optical tomography (DOT) enables us to obtain locally resolved absorption coefficient maps of light-scattering objects without calibrating and with much better resolution than that obtained in DOT.

The point of departure is the well-known diffusion approximation to the radiative transfer equation [6] that is also widely used in DOT [Eq. (1a)]. However, because we now have two sets ("tagged" and "untagged") of measured light fluxes, we can define a second equation [Eq. (1b)], describing specifically the spatial distribution of the US-modulated light flux for cw-mode illumination:

$$\nabla \cdot D(\vec{r})\nabla\phi(\vec{r}) - \mu_a(\vec{r})\phi(\vec{r}) = -S(\vec{r}), \tag{1a}$$

$$\nabla \cdot D(\vec{r})\nabla\phi_m(\vec{r}) - \mu_a(\vec{r})\phi_m(\vec{r}) = -\eta(\vec{r})\phi(\vec{r}), \tag{1b}$$

where $\phi(\vec{r})$ is the photon density distribution created by the incoming light source $S(\vec{r})$, $\phi_m(\vec{r})$ is the modulated photon density, $D(\vec{r})$ describes the light-scattering properties of the medium (for the definition, see e.g., [6]), and $\mu_a(\vec{r})$ is the absorption coefficient. $\eta(\vec{r},t)$ is the US tagging efficiency, which, for simplicity, is assumed to be 1 in the volume occupied by the US focal zone and to be 0 elsewhere. Because of the small frequency shift, the optical properties of the medium are assumed to be identical for modulated and nonmodulated light.

With standard boundary conditions [7], the system can be solved for $\phi(\vec{r})$ using a finite-element method, resulting in the spatial distribution of both US-modulated and nonmodulated light fluxes for a given spatial distribution of scattering and absorption coefficients [8,9]. We are interested in the inverse problem, i.e., the problem in reconstructing a spatially resolved $\mu_a(\vec{r})$ map of the system under investigation on the basis of experimentally available data. In conventional DOT, a set of "measured" light flux values F^M are generated upon rotating the object of interest and minimizing the error function $\chi = \|\{F^M\} - \{F^C(\mu_a)\}\|^2$, where the superscripts ^{M} and ^{C} denote the measured and calculated light fluxes, respectively [10,11]. In the following, we apply this approach to US-modulated photons by using Eq. (1b), and we demonstrate that this leads to a much better spatial resolution of absorbing objects in light-scattering material. Although we consider in this Letter only variations in the absorption coefficient, extension of our approach to variations in the scattering coefficient, albeit with more computational effort, is possible.

In minimizing the error function, the Jacobian J, describing the sensitivity of the measured light fluxes to local variations in the absorption coefficient, plays a decisive role. To demonstrate this, a numerical simulation was performed on a circular scattering medium for a given location of a light source, detector, and US transducer. The results are depicted in Fig. 1, which illustrates a crucial advantage of US-assisted DOT over conventional DOT.

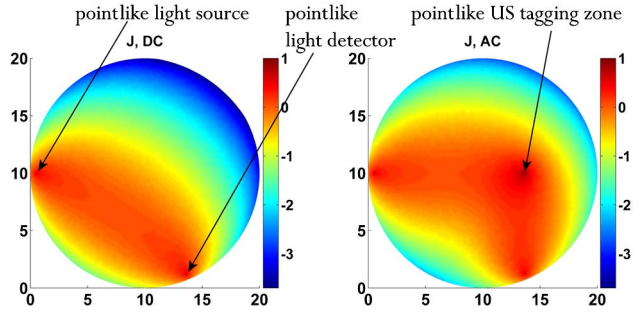

Fig. 1. (Color online) Example of the sensitivity functions (Jacobians, log scale) used in the reconstruction procedure. AC, DC denote the modulated and nonmodulated photon density, respectively. The reduced scattering coefficient of the medium (μ_s') is 1.95 mm^{-1}, and the disk diameter is 20 mm.

The left panel depicts J for the case of a nonmodulated light flux [calculated using Eq. (1a)]; the right panel shows J for the case of a US-modulated light flux [Eqs. (1a) and (1b)]. We see that in the US tagging zone, which can be deep in the scattering medium, J is almost 2 orders of magnitude larger than in the corresponding area of the DOT case. Moreover, the positions of these increased sensitivity regions can be easily adjusted by simply moving around the US tagging zone. In this way, more experimental data are generated and the ratio of known and unknown parameters is increased accordingly. Hence, combined measurements on these various US-irradiated positions are expected to help not only increase the spatial resolution, but also increase the robustness to noise in the measured data. An improvement of the spatial resolution is confirmed by a reconstructed μ_a map in Fig. 2, where a finite-element-based numerical simulation of both an AO-assisted DOT and a DOT experiment is shown.

Encouraged by the results depicted in Fig. 2, we have conducted experiments on a light-scattering sample with embedded absorbing inclusions. Our existing setup [4] was extended to an acousto-optic phase-shifting holography setup [12] by adding a reference beam arm. A computer-controllable rotational stage made this setup a tomography system (see Fig. 3).

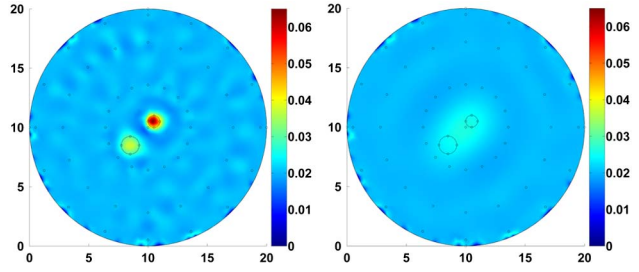

Fig. 2. (Color online) Comparison of recovered absorption images (color scale, in mm^{-1}) using the Levenberg–Marquardt reconstruction algorithm ([10]) for a numerical simulation of (a) AO-assisted DOT, (b) DOT. The number of iterations is 25; light sources\detectors, 16; US-probed positions for AODOT, 5 per angle scan. Preset sizes of the absorbers are 1.5 and 1 mm. Preset μ_a are 0.04 and 0.08 mm^{-1}, respectively. The μ_s' of the surrounding medium is 1.95 mm^{-1}. Large black circles around the image center show the original locations of the absorbers.

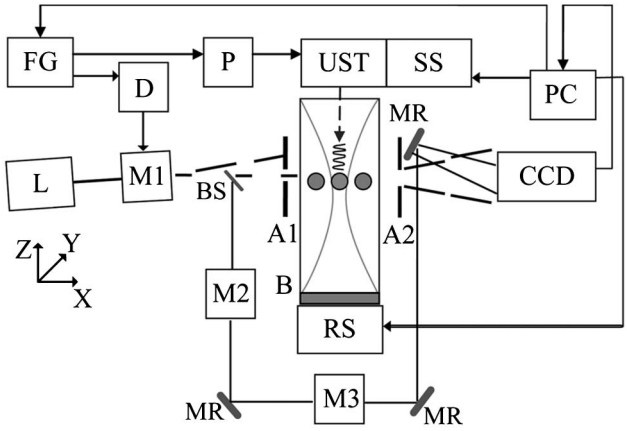

Fig. 3. AODOT setup: FG, two-channel function generator (Tektronix AFG3102); D, delay line; P, MOSFET pulser to drive transducer; UST, 5 MHz US transducer (Panametrics V309); L, cw Ti:sapphire laser (600 mW at $\lambda = 750$ nm), M1–M3, AO modulators (Neos 23080-2); A1, aperture to block nondeflected light; A2, aperture (H × W = 10 mm × 20 mm); B, IL-based phantom; CCD, camera Basler A102f (12 bits, 1392 × 1040); BS, beam splitter; MR, mirrors; RS, rotational stage; SS, scanning stage. In the center of the phantom, the cross section of an absorber-containing tube is depicted. The US propagation is along the Z direction.

To discriminate modulated from nonmodulated light, a Mach–Zehnder interferometer is used. In the reference arm, two acousto-optical modulators (AOMs) upshift the frequency of the light to match the frequency of the US-modulated light, forming a spatially stationary interference pattern on the CCD detector. Basically, this interference pattern is a hologram, and one can apply numerical [fast Fourier transform (FFT)] methods to restore an image of the phantom [12].

To obtain spatially resolved information, a 1 μs US burst with a frequency of 5 MHz was applied to the phantom along the Z axis. Then, after a preset delay time, a 1 μs light pulse, created by deflecting a cw Ti:sapphire laser with AOM M1, strobed the sample. In order to increase the SNR, these US and light pulses were sequentially applied to the phantom with a duty cycle of 25 kHz. So, within 5 ms camera exposure time, 125 pulses were integrated. The distance from the sample surface to the CCD chip was such that the reconstructed image covers the width of the sample along the Y axis. On the recorded fringe pattern, a 2D FFT procedure was applied to produce the intensity profile (image) of the US-modulated light at the output face, bounded by aperture A2. Eight of these images were averaged to improve the SNR. By summing up pixels of the restored image along the Z axis, we obtained the averaged spatially resolved heterodyne intensity along the Y axis. From this averaged heterodyne intensity, having measured the reference arm intensity and the intensity from the sample, we calculated the modulated intensity. By varying the delay time between the US burst and the laser pulse, we can probe the phantom at any position along the Z axis (z scan).

The tissue-mimicking phantom was made of Intralipid in an agar matrix (with $\mu_s' \sim 1.3$ mm^{-1} for $\lambda = 750$ nm, similar to the value of breast tissue), in which three light-absorbing nonscattering inclusions were embedded [see

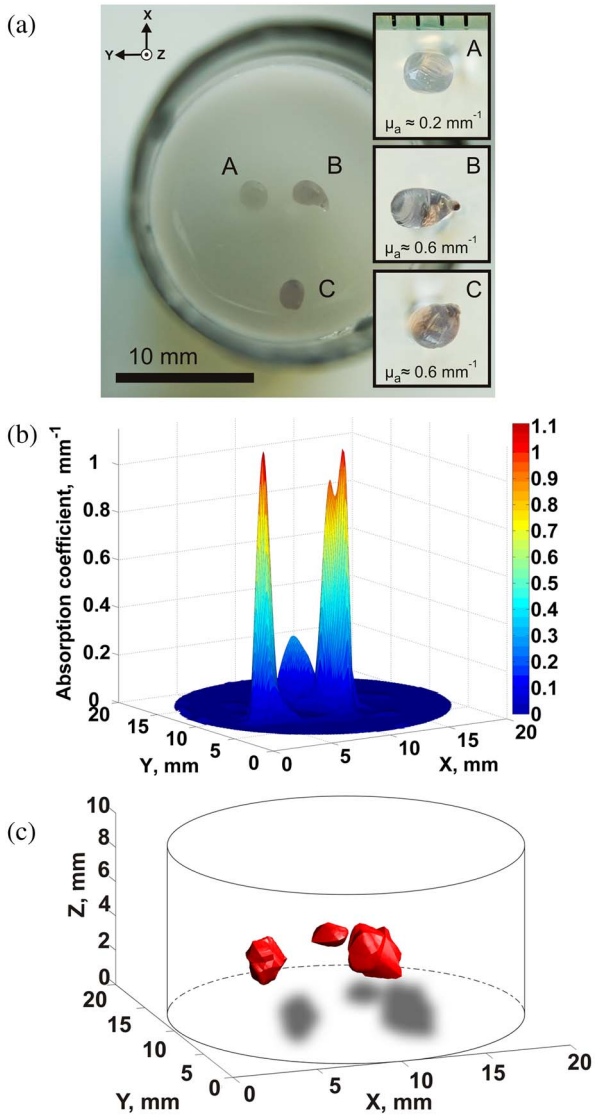

Fig. 4. (Color online) (a) Top view of the image of the phantom (20 mm in diameter), cut at $Z \sim 4$ mm in the XY plane. Absorbing objects (inserts) are ~1.5 mm in diameter. (b) Surface plot for the slice along the XY plane at height of 4.4 mm. Color scale depicts μ_a in mm^{-1}. (c) 3D reconstructed map of the isosurface. The shadows were added afterward, solely for illustration purposes.

Fig. 4(a)]. The phantom was illuminated along the X axis, and the laser beam, the phantom, and the camera axis were positioned approximately in line. To obtain an image with sufficient detail, it sufficed to perform a US x–z scan as follows: the US transducer was moved along the X axis over 11 positions in 1.5 mm steps. At each of these steps, a z scan at three positions was done. When the sequence was finished, the sample was rotated by 10° around the Z axis and the x–z scan was repeated. The measurement procedure was repeated in this manner to cover 360°. A full phantom scan takes ~1 h.

To be able to use the obtained modulated intensity as input for the reconstruction algorithm, we performed a "blank phantom" calibration. In this procedure, the outputs for the case of a homogeneous, nonabsorbing scattering phantom (both from the experiment and the reconstruction algorithm) were equalized, and the derived normalization coefficient was used in further experiments for the experimental data conversion. These measured and converted modulated intensities provided a set of $\mathbf{F}^M$ values, used as input for the error-function minimization procedure. Results of the 3D reconstruction from experimental data for the AO-assisted DOT case are shown in Figs. 4(b) and 4(c). We see that indeed the location and dimensions of the absorbers as well as the absorption coefficients of the inclusions are recovered accurately (the slight overshoot for the case of the absorbers with a high μ_a can be explained by a violation of the condition $\mu_s \gg \mu_a$).

Whereas the use of a 2D model was not able to provide quantitative results (data not shown), the 3D model could also account for the finite dimensions of the US focal zone as well as for the ability of light to propagate above or underneath the absorbers. The obtained spatial resolution of ~1 mm is limited by the 5 MHz 1 μs pulse, as used here. Selecting a higher US frequency will lead to submillimeter resolution.

Based on our results, we expect that AO-assisted DOT can become a powerful technique for noninvasive quantitative investigation of local optical properties of living tissue.

This research was supported by the Technical Science Foundation of the Netherlands project TGT.6656.

References

1. M. Xu and L.-H. V. Wang, Rev. Sci. Instrum. **77**, 041101 (2006).
2. W. Leutz and G. Maret, Phys. B **204**, 14 (1995).
3. L.-H. V. Wang, Dis. Mark. **19**, 123 (2004).
4. A. Bratchenia, R. Molenaar, T. G. van Leeuwen, and R. P. H. Kooyman, J. Biomed. Opt. **14**, 034031 (2009).
5. A. Bratchenia, R. Molenaar, T. G. van Leeuwen, and R. P. H. Kooyman, Appl. Phys. Lett. **92**, 113901 (2008).
6. A. P. Gibson, J. C. Hebden, and S. R. Arridge, Phys. Med. Biol. **50**, R1 (2005).
7. M. Schweiger, S. R. Arridge, M. Hiroaka, and D. T. Delpy, Med. Phys. **22**, 1779 (1995).
8. M. S. Gockenbach, *Understanding and Implementing the Finite Element Method* (SIAM, 2006).
9. M. Schweiger, "Application of the finite element method in infrared image reconstruction of scattering media," Ph.D. thesis (University of London, 1994).
10. P. K. Yalavarthy, B. W. Pogue, H. Dehghani, and K. D. Paulsen, Med. Phys. **34**, 2085 (2007).
11. H. Dehghani, M. E. Eames, P. K. Yalavarthy, S. C. Davis, S. Srinivasan, C. M. Carpenter, B. W. Pogue, and K. D. Paulsen, Commun. Numer. Meth. Eng. **25**, 711 (2009).
12. M. Atlan, B. C. Forget, F. Ramaz, A. C. Boccara, and M. Gross, Opt. Lett. **30**, 1360 (2005).